HHS Public Access

Author manuscript

Clin Biomech (Bristol, Avon). Author manuscript; available in PMC 2018 May 01.

Published in final edited form as:

Clin Biomech (Bristol, Avon). 2017 May ; 44: 36–44. doi:10.1016/j.clinbiomech.2017.03.005.

Novel Mechanical Impact Simulator Designed to Generate Clinically Relevant Anterior Cruciate Ligament Ruptures

Nathaniel A. Bates[1,2,3], **Nathan D. Schilaty**[1,2,3], **Christopher V. Nagelli**[5], **Aaron J. Krych**[1,2], and **Timothy E. Hewett**[1,2,3,4,5]

[1]Department of Orthopedic Surgery, Mayo Clinic, Rochester, MN, USA

[2]Department of Biomedical Engineering and Physiology, Mayo Clinic, Rochester, MN, USA

[3]Sports Medicine Center, Mayo Clinic, Rochester, Minnesota, USA

[4]Department of Physical Medicine & Rehabilitation, Mayo Clinic, Rochester, Minnesota, USA

[5]Department of Biomedical Engineering, The Ohio State University, Columbus, OH, USA

Abstract

Background—Over 250,000 anterior cruciate ligament ruptures occur each year; therefore, it is important to understand the underlying mechanisms of these injuries. The objective of the current investigation was to develop and analyze an impact test device that consistently produces anterior cruciate ligament failure in a clinically relevant manner.

Method—A mechanical impact simulator was developed to simulate the ground reaction force impulse generated from landing in a physiologic and clinically relevant manner. External knee abduction moment, anterior shear, and internal tibial rotation loads were applied to the specimen via pneumatic actuators. The magnitudes of applied loads were determined *in vivo* from a cohort of healthy athletes. Loads were systematically increased until specimen failure was induced. Three cadaveric lower extremity specimens were tested and clinically assessed for failure. Knee specimens were physically and arthroscopically examined at baseline and at post-injury by a board certified orthopedic surgeon.

Findings—All three specimens experienced failure at either the midsubstance or the femoral insertion site. The mean peak strain prior to failure was 18.8 (6.2)%, while the mean peak medial collateral ligament strain was 7.9 (5.9)%.

Corresponding Author: Nathaniel Bates, batesna@gmail.com, Address: Mayo Clinic, 200 First St SW, Rochester, MN, USA 55902.

AUTHOR CONTRIBUTIONS:

Nathaniel Bates: Study design, specimen prep, data collection, data analysis, manuscript preparation
Nathan Schilaty: Study design, specimen prep, data collection, data analysis, manuscript preparation
Christopher Nagelli: Study design, specimen prep, data collection, manuscript preparation
Aaron Krych: Specimen prep, data collection, data analysis, manuscript preparation
Timothy Hewett: Study design, data analysis, manuscript preparation
*All authors have read and approved the final submitted manuscript.

CONFLICTS OF INTEREST: None

Interpretation—A board certified orthopedic surgeon confirmed observed rupture patterns were representative of clinical cases. Peak strains were consistent with literature. The novel mechanical impact simulator will allow researchers to assess clinically relevant patterns of rupture and the data generated will inform clinician decisions. This novel machine presents the ability to assess healthy specimens as well as differences in the function of deficient and reconstructed knees.

Keywords

Anterior cruciate ligament; jump landing; injury simulation; impact; knee ligament biomechanics

1. INTRODUCTION

An overwhelming majority of anterior cruciate ligament (ACL) ruptures occur in non-contact scenarios, typically the result of an impulse force within the first 50 msec of initial ground contact that originate from a rapid deceleration or change of direction.(Agel et al., 2005; Boden et al., 2000; Krosshaug et al., 2006; McNair et al., 1990) Several studies have described various combinations of external knee loads that are involved in ACL injuries. (Boden et al., 2000; Boden et al., 2010; Hewett et al., 2006) In particular, studies have utilized impact-driven mechanical simulators designed to investigate knee biomechanics during simulated jump landings.(Bates et al., 2015a; Hashemi et al., 2010; Levine et al., 2013; Oh et al., 2011; Oh et al., 2012a; Oh et al., 2012, b; Quatman et al., 2014; Withrow et al., 2006a, b) These impact simulators have examined the agonist and antagonist roles of the hamstrings and quadriceps musculature relative to ACL strain.(Bates et al., 2015a) In addition, these simulators have been used to assess the relative influence of induced knee abduction moment (KAM) and internal tibial rotation (ITR) on ligament strain.(Bates et al., 2015a) However, these particular simulators failed to consistently reproduce ACL tears within their cadaveric specimens.(Hashemi et al., 2010; Oh et al., 2011; Oh et al., 2012a; Oh et al., 2012b; Withrow et al., 2006a, 2006b)

A drop-stand mechanical impactor developed by our group was the first impulse simulator to successfully and reliably induce ACL failure on cadaveric specimens.(Kiapour et al., 2012; Levine et al., 2013; Quatman et al., 2014) Of the 17 specimens tested on this machine, 15 sustained an ACL disruption.(Levine et al., 2013) While previous impact simulators demonstrated both ITR and KAM contributed to increased peak ACL strain, the first generation drop-stand impactor showed that only knee abduction moment (KAM) significantly contributed to calculated ACL strain at failure.(Levine et al., 2013) However, despite its success in the creation of ACL injuries, the first generation drop-stand impactor had limitations. Bony injury severity was often greater than that observed in the operating room, which may indicate that greater magnitudes of loading were applied to the impactor specimens than *in vivo*.(Levine et al., 2013) Also, tibial avulsion failures, which are more common in cadaveric tissue than *in vivo* cases, were observed in 4 of 15 cases, while tears at the tibial insertion were observed in an additional 5 of 15 cases.(Levine et al., 2013) Thus, although ACL ruptures occurred in the cadaveric specimens, they failed to reproduce the physical distribution of ACL rupture location within the ligament structure that is typically observed in the clinical setting. Therefore, augmentation of the current simulator design to

produce more clinically relevant injury patterns may provide further insight into injury ACL mechanisms. (Meyer et al., 2008)

The objective of the current investigation was to develop and analyze an impact test device that produces ACL ruptures on cadaveric specimens in a manner that reproduces the patterns of failure seen in the clinical environment. It was hypothesized that the design modifications made to the external load and muscle force application from the previous generation impactor device would lead to ACL ruptures that are more consistent with the clinically observed patterns of ACL injury.

2. METHODS

2.1 Mechanical Design

The mechanical impact simulator is a gravity-driven mechanical testing apparatus designed to generate impulse forces at the knee on lower extremity joints that are representative of the *in vivo* loading induced when landing from a jump. It was designed around the utilization of two weight sleds on a minimal-friction, slide-rail track system to deliver an impact load to the foot of an inverted lower extremity specimen (Figure 1). The inferiorly positioned weight sled served as the ground, resting on the base of a specimen's foot, while the superiorly positioned sled was suspended by electromagnets 31 cm above the ground sled. Modifications unique to the presented impactor include an electrical trigger that was used to release the drop sled from the electromagnets, allowing it to fall along the slide-rail track solely with gravitational force and impact the prepared specimen in alignment to the tibial shaft. Additionally, apart from the impact load, external forces and torques associated with ACL loading were applied about the knee with pneumatic actuators to simulate various degrees of relative injury risk loading on each specimen. Investigational methods were approved by the Institutional Review Board at Mayo Clinic.

2.2 Specimen Preparation

Three (3) cadaveric full lower extremity specimens from unique donors (age = 33.0 (13.1) years [min = 24, max = 48]; mass = 90.1 (28.1) kg) were obtained from an anatomical donations program (Anatomy Gifts Registry, Hanover, MD) to validate our methodology. Specimens over 50 years of age and those with previous history of knee trauma or knee surgery were excluded from this investigation. The specimens were kept frozen at −20° C until 24 hours prior to use. After thawing, specimens were prepared to be mounted into the mechanical impact simulator. The skin 5 cm proximal to the superior aspect of the patella was resected and thigh musculature was individually isolated. The quadriceps, biceps femoris, semitendinosus, semimembranosus, and gracilis tendons were identified and rasped to remove muscle tissue leaving the tendinous tissue intact. All other musculature was resected. The femur was then resected 20 cm proximal to the superior patella and the distal end of the femur was potted with Bondo® aligned with the long axis of the bone in a 2-inch inner diameter cylinder. The quadriceps tendon was then aligned with and placed into a cable clamp and secured with a U-bolt such that tension could be applied along the loading axis of the tendon. This process was similarly completed two additional times with the

semimembranosus, semitendinosus, and gracilis groups on the medial aspect of the posterior knee and the biceps femoris on the lateral aspect of the posterior knee (Figure 1).

Once the femoral shaft was potted, a custom-designed external fixation frame was rigidly mounted to the shank of the specimen (Figure 2).(Kiapour et al., 2012; Levine et al., 2013; Quatman et al., 2014) Briefly, a hollow steel rod halved length-wise was affixed to the anterior and posterior aspect of the lower leg beginning just distal to the tibial tubercle and continuing distally toward the ankle. Carriage bolts were placed through pre-drilled holes through both superior and inferior aspects of the halved rods and tibia. These bolts were secured in place to form a compression clamp around the tibia. Two half-circle aluminum mounts were bolted onto the anterior aspect of the hollow steel rod. The more proximal aluminum mount was affixed with steel bars that protruded medially and laterally from the shank and were used to apply external anterior tibial shear (ATS) and ITR. The more distal aluminum mount was affixed with grooved polymer disks that were positioned anteriorly and posteriorly to the shank and were used to apply external KAM. The rigid fixation of this tibial frame was designed such that the points of load application were located about the approximate knee joint center.

Dual incisions were made on the anteromedial and anterolateral aspects of the knee capsule on the side of the patellar tendon to serve as ports into the internal knee. Ligament integrity was confirmed via an arthroscopic lens (Stryker Corporation, Kalamazoo, MI). The knee was then articulated through a passive flexion range of motion to evaluate for possible impingement of the anteromedial bundle of the ACL on femoral notch. If impingement was observed, a femoral notchplasty was performed with a burr (Stryker Corporation, Kalamazoo, MI) by a biomechanics researcher that was trained by an orthopedic surgeon. Subsequently, a custom-barbed 3 mm microminiature differential variable strain transducer (DVRT, LORD MicroStrain, Willingston, VT) was implanted on the anteromedial bundle of the ACL as previously described in the literature.(Fleming et al., 1994; Levine et al., 2013; Quatman et al., 2014) In addition, an incision on the medial knee was made to implant a DVRT on the medial collateral ligament (MCL). With the DVRTs implanted, the specimen was again articulated through the knee range of motion to verify no impingement was present between the femoral notch and DVRT. If impingement was identified, additional bony tissue was burred from the notch and sensor placement and impingement verification repeated.

2.3 Specimen mounting

The prepared specimen was inverted and the Bondo® mounting cylinder encasing the proximal femur was inserted into a custom-fitted stainless steel potting cup that aligned the long axis of the femur with the primary loading axis of a 6-axis load cell (Omega160 IP65/IP68, ATI Industrial Automation, Inc., Apex, NC, USA). The mounting cylinder was rigidly secured in place with eight perpendicular setscrews that apply pressure through the potting cup. This potting cup was affixed directly to the load cell, such that any forces that propagated through the femur would also propagate through the load cell. The concept applied here was utilized in the previous drop-stand impactor as well as in robotic models of knee joint articulation.(Bates et al., 2015b; Kiapour et al., 2012; Levine et al., 2013;

Quatman et al., 2014) This potting cup / load cell assembly was rigidly secured such that the long axis of the femur was oriented at a 25° with the vertical plane. A knee flexion angle of 25° is representative of initial contact knee orientation in young athletes landing from a drop height of 31 cm.(Bates et al., 2013; Koga et al., 2010) The potting cup / load cell assembly was suspended above the ground such that the tibial alignment could be adjusted rotationally in the frontal and transverse planes, as well as translationally along the medial/lateral and anterior/posterior axes.

The cable clamps affixed to the hamstrings and quadriceps tendons were then attached to pneumatic actuators (CG5LN40SV-100 and CG5LN50SV-100, SMC Corporation, Tokyo, Japan) via carbon fiber rope ($Ø^{7}/_{64}$ in.; Amsteel®-Blue, Samson, Ferndale, WA, USA). These pneumatic cylinders are unique to this impactor and were custom mounted to the aforementioned potting cup and used to apply 450 N pre-tensioning to the quadriceps tendon and 225 N pre-tension to both hamstrings tendon groups (Figure 3). The force applied by the quadriceps and hamstrings mounted pneumatic actuators was maintained constant throughout the testing process. An ideal activation ratio between hamstrings and quadriceps muscles relative to injury risk is 1:1.(Myer et al., 2009) Athletes who demonstrate a hamstrings to quadriceps ratio of less than 0.6 predispose themselves to increased injury risk, as the quadriceps serve an antagonistic role to the ACL by increasing ATS during contraction.(Hewett et al., 2004; Hewett et al., 1996; Myer et al., 2009; Renstrom et al., 1986) Meanwhile, the hamstrings serve an agonist role by actively counteracting this ATS. (Renstrom et al., 1986) The carbon fiber robe from each pneumatic muscle actuator was run through a pulley, to orient it in a direction representative of physiologic line of action that corresponds with each respective tendon *in vivo*.

Five additional pneumatic actuators were attached to various points on the custom tibial fixture. These attachment points corresponded with the static weight attachments of previous drop-stand impactors and are documented in the literature.(Kiapour et al., 2012; Levine et al., 2013; Quatman et al., 2014) Briefly, two pneumatic cylinders (MQQTL40TN-100DM, SMC Corporation, Tokyo, Japan) were mounted anterior to the medial and lateral sides of the specimen and apply ATS in equal amounts. A single cylinder (MQQTL40TN-100DM, SMC Corporation, Tokyo, Japan) was mounted posteromedial to the specimen and applied additional load in conjunction with the anterolateral pneumatic to create coupled ITR. Finally, two additional pneumatic cylinders (CG5LN80SV-100, SMC Corporation, Tokyo, Japan) were mounted to the medial and lateral aspect of the knee joint. These cylinders were affixed to parallel cylindrical bodies mounted to the anterior and posterior aspect of the tibial fixture and their actuation allowed for coupled generation of KAM. All of the external load pneumatic actuators were activated prior to the electromagnetic weight sled release. This allowed each actuator to ramp up to the peak desired force immediately prior to instantaneous impact of the drop sled and then relax following each trial (Figure 3). Following each trial the pneumatic loads were released and the specimen was able to return to its neutral position. This near instantaneous application and relaxation of external loads to the cadaveric joint is unique to the presented impactor and reduces the limitation of tissue and orientation creep introduced by the extended duration of load application seen in previous landing simulators.

Once the external load applicators were connected, the tibia was aligned vertically and a free-sliding platform mounted to the slide rails was lowered onto the sole of the foot. This platform contained a uniaxial load cell (1720ACK-10kN, Interface, Inc., Scottsdale, AZ, USA), which was aligned, on its inferior side, with the vertical axis of the tibia going through the heel of the specimen and was aligned, on its superior side, with the center of mass point of impact from the drop sled. The prescribed alignment permitted the load cell to measure the impulse force delivered from the drop sled to the specimen upon impact. This allows for direct quantification of impulse force transfer between the impact sled and test specimen. (Kiapour et al., 2012; Levine et al., 2013; Quatman et al., 2014)

2.4 Testing protocol

The three external load variables (KAM, ATS, and ITR) were adjusted relative to *in vivo* motion analysis data that was previously captured and analyzed from a cohort of 67 healthy adolescent and young adult athletes (age = 23.2 (3.9) years; mass = 73.3 (13.4) kg) with IRB approval at The Ohio State University Sports Health and Performance Institute. Using a modified Helen Hayes marker set, each athlete was instrumented with 55 retroreflective skin markers positioned at anatomical landmarks (C7, right and left acromion, right and left upper arm, right and left elbow, right and left wrist, clavicular notch, right and left posterior trunk, distal posterior trunk, T12, L2, right and left lower back, right and left PSIS, right and left ASIS, sacrum, posterior offset, right and left greater trochanter, right and left superior thigh, right and left inferior thigh, right and left anterior thigh, right and left distal thigh, right and left lateral knee, right and left medial knee, right and left tibial tubercle, right and left mid shank, right and left distal tibia, right and left lateral ankle, right and left medial ankle, right and left heel, right and left posterior foot, right and left lateral foot, right and left toe). The markers were placed by a single, trained investigator.(Ford et al., 2003, 2007) The three trunk markers were pre-placed on a backpack that was tightened around the torso of the subject (CamelBak Products, LLC, Petaluma, CA, USA). Likewise, four markers were pre-placed on predetermined footware (Air Pegasus 28, Nike Inc., Beaverton, OR, USA) that was matched to each subject's shoe size. Marker positional data was collected continuously at 240 Hz across three drop vertical jump (DVJ) trials for each subject using a 12-camera motion analysis system (Raptor-12 cameras, Motion Analysis Corporation, Santa Rosa, CA). Ground reaction forces were recorded at 10 kHz by dual, in-ground, 6-axis force platforms (FP6090-15-2000, Bertec Corporation, Columbus, OH, USA). Marker positional data and ground reaction force data were filtered through a low-pass Butterworth filter at 6 Hz and 50 Hz, respectively. The data was then fed into biomechanical modeling software (Visual3D, version 5, C-motion Inc., Germantown, MD, USA) where a custom model was employed to calculate joint kinetics and kinematics. Specimens were subjected to a series of impact tests that consisted of both sub-failure and failure loading determined from the kinetics reported from this *in vivo* cohort. For the sub-failure protocol, specimens were run through a randomized order of 46 impact tests with a constant drop sled weight (75 lbs) and varying magnitudes of KAM, ATS, and ITR matched to the corresponding *in vivo* kinetics recorded for the 1^{st}, 33^{rd}, and 67^{th} percentile of the population cohort (Table 1). These percentiles of loading were then randomized across each variable until all combinations were tested (27 impacts; Table 2). The same process was then repeated for the 33^{rd}, 67^{th}, and 100^{th} percentile, with the exclusion of those tests that had already been conducted (19 impacts).

Once the sub-failure protocol was completed, the failure protocol was initiated. For failure testing, the drop sled weight was adjusted to be specimen specific at 0.5*bodyweight. KAM, ATS, and ITR were then each adjusted to the 100th percentile loading from the *in vivo* cohort and an impact was performed. For each ensuing impact, the drop sled weight remained constant at 0.5*bodyweight while the KAM, ATS, and ITR loads were simultaneously increased in magnitude by 20%. This protocol was followed until the specimen demonstrated a tangible soft or hard tissue failure (Table 3). At baseline, the knee specimens were examined by a board certified orthopedic surgeon to ensure no ligament damage. Following failure, each specimen was assessed clinically and arthroscopically for damage by the same surgeon. Care was taken to document the type and location of injuries to the cruciate ligaments, collateral ligaments, articular cartilage, bony structures, and menisci.

2.5 Data collection

The six-axis ATI load cell reported whole knee joint forces and torques in all six degrees of freedom relative to the joint center point. The uniaxial Interface load cell reported the vertical ground reaction force (vGRF) impulse generated by the impact of the drop sled and the specimen foot. A uniaxial tension load cell (MLP-300 or MLP-1K, Transducer Techniques, Temecula, CA) was affixed to the end effector of each pneumatic cylinder. These cells recorded the individual linear force output from each pneumatic. The DVRTs implanted on the ACL and MCL recorded ligament strain. Absolute strains were calculated with established methods that compare instantaneous ligament length with a distinct inflection point in the DVRT force-displacement curve.(Kiapour et al., 2012; Levine et al., 2013; Quatman et al., 2014) As the instantaneous loading and rupture of the ACL made the precise moment of failure indeterminable in many cases, the peak ACL strain from the impact that immediately preceded ligament damage was documented. Damage was identified by a significant change or complete absence of elastic behavior in the ACL as recorded by the DVRT sensors. Collection of all dependent variables were synced via electronic trigger and sampled continuously at 10 kHZ throughout each impact trial (unless otherwise noted).

Following testing, a board certified orthopedic surgeon performed clinical evaluations to assess the functional integrity of intraarticular knee structures. A Lachman’s test, anterior drawer test, posterior drawer test, and medial laxity evaluation were performed and scored on a clinical scale from grade 0 (normal) to grade 3 (ruptured, nonfunctional). Specifically, grade 1 was defined as 5 mm laxity, grade 2 was 5 to 10 mm laxity, and grade 3 greater than 10 mm laxity.

3. RESULTS

All three specimens tested survived the prescribed sub-failure protocol. However, during the failure protocol we successfully induced ACL disruptions. A board certified orthopedic surgeon affirmed that all three specimens tested experienced ACL rupture during the failure protocol in a manner consistent with patterns that are observed clinically (Table 3, Figure 4).

The external load actuators reached peak magnitude prior to impact (Figure 3). The vGRF impulse was independent of external loading and consistent throughout all test (Figure 5).

For each impact trial on an intact specimen, the DVRT sensors on the ACL depicted an acute and immediate increase in ligament strain (Figure 6). For impact trials where the ACL remained intact, this acute strain impulse was followed by a relaxation. During trials where failure occurred, this elastic rebound was not observed (Figure 6). ACL strain increased in magnitude from the condition where external pneumatic actuators for KAM, ITR, and ATS replicated loads representative of the 0^{th} percentile of the *in vivo* population to the condition where external pneumatics replicated loads representative of the 100^{th} percentile of the *in vivo* population (Figure 7). The mean peak ACL strain leading up to failure was 18.8 (6.2)% with a range of 14.4% – 25.9%. ACL failure was confirmed with a grade 3 anterior laxity and Lachman's test in all specimens.

The impact testing did not cause arthroscopically-identifiable damage to any intra-articular knee structures apart from the ACL. For each impact trial, the DVRT sensors on the MCL depicted and acute, immediate increase in ligament strain, which was followed by an elastic relaxation. There were no visible MCL failures following specimen failure. However, post-testing clinical examination did reveal medial laxity in the knee (Table 3). At the time of ACL failure, the average peak MCL strain was 7.9 (5.9)% with a range of 1.9% – 13.8% (Figure 8).

4. DISCUSSION

The hypothesis that the novel mechanical impact simulator would lead to ACL ruptures that are consistent with the clinically observed patterns of ACL injury was supported. The most frequently observed location of ACL rupture in adolescent athletes is at or near the femoral insertion.(Kocher et al., 2002) Intra-substance tears are the second most common location of clinical ACL ruptures, while patients less frequently present with tibial side tears. Impact-driven simulators have previously demonstrated that increased ATS and KAM applied to the knee correspond with increased strain on the ACL during landing.(Withrow et al., 2006a, b) However, those particular simulations were not designed to rupture the ACL. Our previous drop-tower impactor was able to rupture the ACL in 88% of specimens tested, but the location of these failures trended toward the tibial aspect of the ligament as compared to the more femoral location of *in vivo* ruptures.(Levine et al., 2013) All three specimens piloted in the presently-described mechanical impact simulator experienced complete ACL disruption near the femur. These injury locations better resemble clinically observed patterns of ACL disruption.

The mechanical impact simulator described in this paper utilized pneumatics to actuate muscle loads and external forces acting on the lower extremity specimen. In comparison to the inertia from static hanging weights, pneumatic pistons are advantageous because their pressurized cylinders provide a greater element of dampening against the sudden impulse load enacted on a specimen during impact. This behavior can be seen in Figure 3. When impulses are applied *in vivo*, muscles actively work to rapidly dampen perturbation and

vibration in an effort to maintain the body's positional equilibrium. Thus, the adaptation of pneumatics improved the physiological relevance of the mechanical impact simulator.

The presently reported mechanical impact simulator positioned the muscle pneumatic actuators, and their corresponding pulleys, superior to the 6-axis load cell, along with the cadaveric specimen. If the tension wires were to traverse the compressive loading axis of the load cell, there would be potential for artifact generation in the compressive degree of freedom. It can be observed that, though the two hamstrings and one quadriceps actuator were active for the entire duration of the recorded impact simulation, no forces were registered by the 6-axis load cell until after the external knee load pneumatic actuators engaged (Figure 3). Therefore, the present model confirms that compressive loading artifacts were not present. Additionally, the 6-axis ATI load cell was zeroed prior to each trial to compensate for any loading artifacts that would be created by the mass of the mounted pneumatics.

The device used slide rails and reduction in the footprint of the simulator. Three-quarter inch slide rails were used to guide the fall of the impact sled. These greased rods were precisely manufactured and provided minimal friction resistance, which allowed the drop sled to accelerate at a rate as close to natural gravity as possible. The physiologic advantage was that the mechanical impactor accelerated its mass at near the same rate an athlete would accelerate when landing from a jump. Thus, the mechanical impact simulator is capable of delivering physiologic landing impulses customizable to any predetermined fall height and mass.

The ligament strains reported in this preliminary data from the mechanical impact simulator are consistent with previous literature. Peak ACL strain prior to failure was reported as 18.8 (6.2)% in the present investigation, which is nearly identical to the 18.7 (10.0)% reported previously by our group.(Levine et al., 2013) This is also comparable to middle aged specimens that failed at 15.0% strain when uniaxially loaded along the ACL.(Butler et al., 1986) Peak MCL strain in the current investigation was well below the previously reported failure threshold of 17.1% and 17.6% in uniaxial loading.(Bates et al., 2015c; Quapp and Weiss, 1998) This fact exhibits that the ACL is susceptible to rupture without concomitant injury to the MCL and supports why only 30% of ACL injuries also incur MCL damage. (LaPrade et al., 2007; Sankar et al., 2006) The concept of disproportionate ACL:MCL load ratios is supported as robotic simulation demonstrated an ACL:MCL strain ratio of 15.3 for DVJ and 10.8 for sidestep cutting tasks and impact simulation demonstrated an ACL:MCL strain ration of 1.7.(Bates et al., 2015c; Quatman et al., 2014) The present impact method likewise demonstrated an ACL:MCL strain ratio of 2.4.

While we have demonstrated that the mechanical impact simulator can recreate clinically relevant ACL tears, the device is not without limitations. The current design applies constant force muscle actuations to bundles of the hamstrings and quadriceps tendons. *In vivo*, each muscle body would actuate its own unique load on the lower extremity, and these forces would not be constant throughout motion. Further, only two muscle groups are accounted for in the present model, leaving much of the lower extremity musculature inactive. However, relative hamstrings and quadriceps activation ratios encompass the muscle activations that

are most directly associated with ACL injury risk and, therefore, most applicable to the purpose of the present simulations.(Hewett et al., 2004; Hewett et al., 1996; Myer et al., 2009; Renstrom et al., 1986; Withrow et al., 2006b, 2008) Secondly, in the present simulation, the knee flexion angle is locked at 25°. This orientation was selected because video analysis has demonstrated that ACL injury occurs within the first 50 ms of initial ground contact when the knee flexion is ≤ 25°.(Krosshaug et al., 2006) *In vivo*, athletes would have the added ability to flex their knees upon landing as compared to the present *in vitro* specimens. However, it is postulated that landing flat-footed in a stiff, extended knee posture is a potential precursor to ACL injury.(Hewett et al., 1999; Hewett et al., 2005; Hewett et al., 2009)

CONCLUSIONS

We developed and executed a novel mechanical impact simulator that was confirmed, by an orthopedic surgeon, to create clinically representative patterns of ACL failure on cadaveric lower extremity specimens. Additionally, the ACL failure mechanics observed were consistent with the literature, while several limitations that inhibited previous simulators were addressed. Thus, the mechanical impact simulator was optimized for the evaluation and study of clinical ACL injuries in cadaveric specimens. This device also exhibits the potential to assess how ACL deficient and ACLR conditions influence intra-articular function of the knee. The clinically relevant data generated during these impactor experiments has the potential to inform clinician decisions related to injury prevention, ACLR, and rehabilitation.

Acknowledgments

The authors acknowledge the support of the staff at the Materials Structural Testing CORE at Mayo Clinic, the Biomechanics Research Lab at Mayo Clinic, the Sports Health and Performance Institute at The Ohio State University. The authors acknowledge funding from NIH grants R01AR049735, R01AR056259, R01AR055563, T32AR056950, and L30AR070273.

References

Agel J, Arendt EA, Bershadsky B. Anterior cruciate ligament injury in national collegiate athletic association basketball and soccer: a 13-year review. Am J Sports Med. 2005; 33:524–530. [PubMed: 15722283]

Bates NA, Ford KR, Myer GD, Hewett TE. Kinetic and kinematic differences between first and second landings of a drop vertical jump task: Implications for injury risk assessments. Clin Biomech. 2013

Bates NA, Myer GD, Shearn JT, Hewett TE. Anterior cruciate ligament biomechanics during robotic and mechanical simulations of physiologic and clinical motion tasks: A systematic review and meta-analysis. Clin Biomech. 2015a; 30:1–13.

Bates NA, Nesbitt RJ, Shearn JT, Myer GD, Hewett TE. A Novel Methodology for the Simulation of Athletic Tasks on Cadaveric Knee Joints with Respect to In Vivo Kinematics. Ann Biomed Eng. 2015b; 43:2456–2466. [PubMed: 25869454]

Bates NA, Nesbitt RJ, Shearn JT, Myer GD, Hewett TE. Relative strain in the anterior cruciate ligament and medial collateral ligament during simulated jump landing and sidestep cutting tasks: implications for injury risk. Am J Sports Med. 2015c; 43:2259–2269. [PubMed: 26150588]

Boden BP, Dean GS, Feagin JA, Garrett WE. Mechanisms of anterior cruciate ligament injury. Orthopedics. 2000; 23:573–578. [PubMed: 10875418]

Boden BP, Sheehan FT, Torg JS, Hewett TE. Noncontact anterior cruciate ligament injuries: mechanisms and risk factors. J Am Acad Orthop Surg. 2010; 18:520–527. [PubMed: 20810933]

Butler DL, Kay MD, Stouffer DC. Comparison of material properties in fascicle-bone units from human patellar tendon and knee ligaments. J Biomech. 1986; 19:425–432. [PubMed: 3745219]

Fleming BC, Beynnon BD, Tohyama H, Johnson RJ, Nichols CE, Renstrom P, Pope MH. Determination of a Zero Strain Reference for the Anteromedial Band of the Anterior Cruciate Ligament. J Orthop Res. 1994; 12:789–795. [PubMed: 7983554]

Ford KR, Myer GD, Hewett TE. Valgus knee motion during landing in high school female and male basketball players. Med Sci Sports Exerc. 2003; 35:1745–1750. [PubMed: 14523314]

Ford KR, Myer GD, Hewett TE. Reliability of landing 3D motion analysis: implications for longitudinal analyses. Med Sci Sports Exerc. 2007; 39:2021–2028. [PubMed: 17986911]

Hashemi J, Breighner R, Jang TH, Chandrashekar N, Ekwaro-Osire S, Slauterbeck JR. Increasing pre-activation of the quadriceps muscle protects the anterior cruciate ligament during the landing phase of a jump: an in vitro simulation. Knee. 2010; 17:235–241. [PubMed: 19864146]

Hewett TE, Lindenfeld TN, Riccobene JV, Noyes FR. The effect of neuromuscular training on the incidence of knee injury in female athletes. A prospective study. Am J Sports Med. 1999; 27:699–706. [PubMed: 10569353]

Hewett TE, Myer GD, Ford KR. Decrease in neuromuscular control about the knee with maturation in female athletes. J Bone Joint Surg Am. 2004; 86-A:1601–1608. [PubMed: 15292405]

Hewett TE, Myer GD, Ford KR. Anterior Cruciate Ligament Injuries in Female Athletes: Part 1, Mechanisms and Risk Factors. Am J Sports Med. 2006; 34:299–311. [PubMed: 16423913]

Hewett TE, Myer GD, Ford KR, Heidt RS Jr, Colosimo AJ, McLean SG, van den Bogert AJ, Paterno MV, Succop P. Biomechanical Measures of Neuromuscular Control and Valgus Loading of the Knee Predict Anterior Cruciate Ligament Injury Risk in Female Athletes: A Prospective Study. Am J Sports Med. 2005; 33:492–501. [PubMed: 15722287]

Hewett TE, Stroupe AL, Nance TA, Noyes FR. Plyometric training in female athletes. Decreased impact forces and increased hamstring torques. Am J Sports Med. 1996; 24:765–773. [PubMed: 8947398]

Hewett TE, Torg JS, Boden BP. Video analysis of trunk and knee motion during non-contact anterior cruciate ligament injury in female athletes: lateral trunk and knee abduction motion are combined components of the injury mechanism. Br J Sports Med. 2009; 43:417–422. [PubMed: 19372088]

Kiapour, AM., Quatman, CE., Goel, VK., Levine, JW., Wordeman, SC., Hewett, TE., Demetropoulos, CK. A novel technique to simulate landing biomechanics: a cadaveric model of ACL injury. Orthopaedic Research Society; San Francisco, CA, USA: 2012.

Kocher MS, Micheli LJ, Zurakowski D, Luke A. Partial tears of the anterior cruciate ligament in children and adolescents. Am J Sports Med. 2002; 30:697–703. [PubMed: 12239005]

Koga H, Nakamae A, Shima Y, Iwasa J, Myklebust G, Engebretsen L, Bahr R, Krosshaug T. Mechanisms for noncontact anterior cruciate ligament injuries: knee joint kinematics in 10 injury situations from female team handball and basketball. Am J Sports Med. 2010; 38:2218–2225. [PubMed: 20595545]

Krosshaug T, Nakamae A, Boden BP, Engebretsen L, Smith G, Slauterbeck JR, Hewett TE, Bahr R. Mechanisms of Anterior Cruciate Ligament Injury in Basketball: Video Analysis of 39 Cases. Am J Sports Med. 2006

LaPrade RF, Wentorf FA, Fritts H, Gundry C, Hightower CD. A prospective magnetic resonance imaging study of the incidence of posterolateral and multiple ligament injuries in acute knee injuries presenting with a hemarthrosis. Arthroscopy. 2007; 23:1341–1347. [PubMed: 18063179]

Levine JW, Kiapour AM, Quatman CE, Wordeman SC, Goel VK, Hewett TE, Demetropoulos CK. Clinically relevant injury patterns after an anterior cruciate ligament injury provide insight into injury mechanisms. Am J Sports Med. 2013; 41:385–395. [PubMed: 23144366]

McNair PJ, Marshall RN, Matheson JA. Important features associated with acute anterior cruciate ligament injury. N Z Med J. 1990; 103:537–539. [PubMed: 2243642]

Meyer EG, Baumer TG, Slade JM, Smith WE, Haut RC. Tibiofemoral contact pressures and osteochondral microtrauma during anterior cruciate ligament rupture due to excessive compressive loading and internal torque of the human knee. Am J Sports Med. 2008; 36:1966–1977. [PubMed: 18490469]

Myer GD, Ford KR, Barber-Foss K, Liu C, Nick TG, Hewett TE. The relationship of hamstrings and quadriceps strength to anterior cruciate ligament injury in female athletes. Clinical Journal of Sports Medicine. 2009; 19:3–8.

Oh YK, Kreinbrink JL, Ashton-Miller JA, Wojtys EM. Effect of ACL Transection on Internal Tibial Rotation in an in Vitro Simulated Pivot Landing. J Bone Joint Surg Am. 2011; 93:372–380. [PubMed: 21325589]

Oh YK, Kreinbrink JL, Wojtys EM, Ashton-Miller JA. Effect of axial tibial torque direction on ACL relative strain and strain rate in an in vitro simulated pivot landing. J Orthop Res. 2012a; 30:528–534. [PubMed: 22025178]

Oh YK, Lipps DB, Ashton-Miller JA, Wojtys EM. What strains the anterior cruciate ligament during a pivot landing? Am J Sports Med. 2012b; 40:574–583. [PubMed: 22223717]

Quapp KM, Weiss JA. Material characterization of human medial collateral ligament. J Biomech Eng. 1998; 120:757–763. [PubMed: 10412460]

Quatman CE, Kiapour AM, Demetropoulos CK, Kiapour A, Wordeman SC, Levine JW, Goel VK, Hewett TE. Preferential loading of the ACL compared with the MCL during landing: a novel in sim approach yields the multiplanar mechanism of dynamic valgus during ACL injuries. Am J Sports Med. 2014; 42:177–186. [PubMed: 24124198]

Renstrom P, Arms SW, Stanwyck TS, Johnson RJ, Pope MH. Strain within the anterior cruciate ligament during hamstring and quadriceps activity. Am J Sports Med. 1986; 14:83–87. [PubMed: 3752352]

Sankar WN, Wells L, Sennett BJ, Wiesel BB, Ganley TJ. Combined anterior cruciate ligament and medial collateral ligament injuries in adolescents. J Pediatr Orthop. 2006; 26:733–736. [PubMed: 17065935]

Withrow TJ, Huston LJ, Wojtys EM, Ashton-Miller JA. The effect of an impulsive knee valgus moment on in vitro relative ACL strain during a simulated jump landing. Clin Biomech. 2006a; 21:977–983.

Withrow TJ, Huston LJ, Wojtys EM, Ashton-Miller JA. The relationship between quadriceps muscle force, knee flexion, and anterior cruciate ligament strain in an in vitro simulated jump landing. Am J Sports Med. 2006b; 34:269–274. [PubMed: 16260464]

Withrow TJ, Huston LJ, Wojtys EM, Ashton-Miller JA. Effect of varying hamstring tension on anterior cruciate ligament strain during in vitro impulsive knee flexion and compression loading. J Bone Joint Surg Am. 2008; 90:815–823. [PubMed: 18381320]

HIGHLIGHTS

- Simulator executed physiologic landing forces on cadaveric lower extremities.
- Applied *in vivo* knee kinetics to mimic relative anterior cruciate ligament injury risk.
- Specimens experienced anterior cruciate ligament failure with high risk biomechanics.
- Ligament failures occurred proximally near femoral insertion (clinical pattern).
- First ligament injury simulator to consistently generate failure in clinical location.

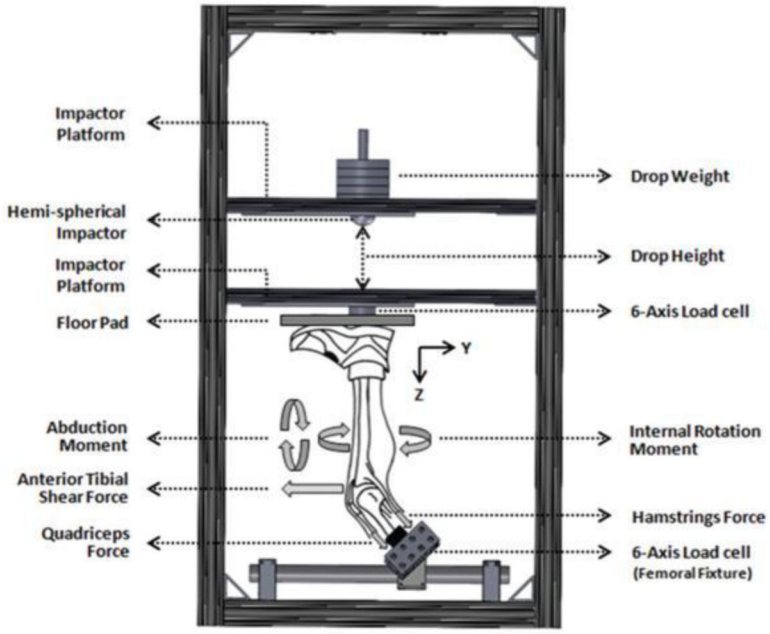

Figure 1.

Custom designed landing impact test apparatus. Image reproduced with permission from Quatman, et al. *Am J Sports Med*, 2014, 42(1):177–186.

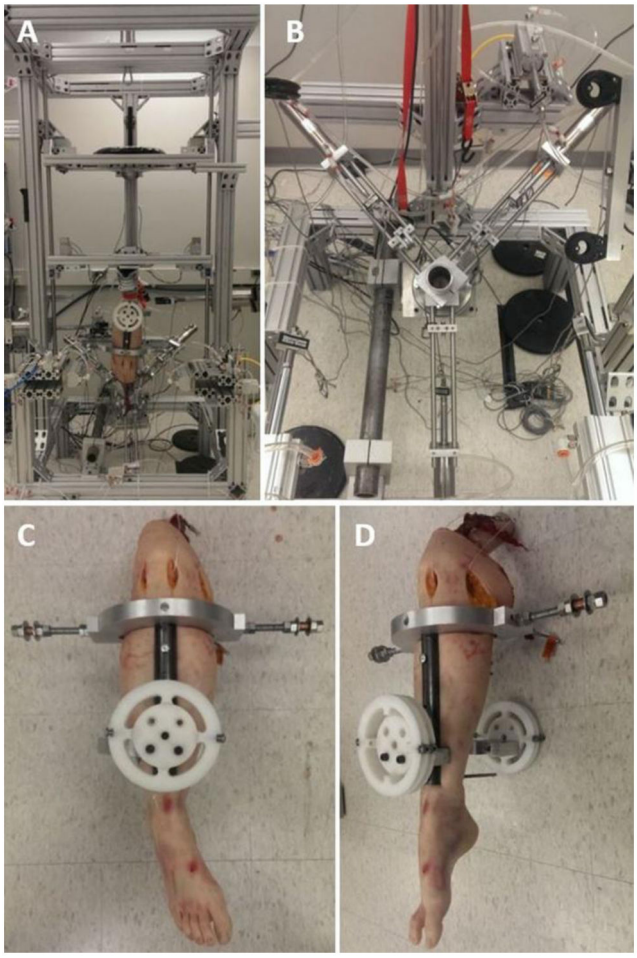

Figure 2.

Depiction of the mechanical impactor simulator. (A) Frontal view of the entire apparatus with a mounted specimen. Pneumatic actuators to apply external load can be seen mounted on the front and side aspects of the simulator structure. (B) Top view of the 6-axis load cell, potting cut, and muscle actuator assembly. The quadriceps actuator is at the inferior aspect of the image while the hamstrings actuators are in the superior corners of the image. (C) Frontal view of the tibial fixture mounted on a specimen. KAM is affixed and applied to the circular rotary elements pictured, while ATS and ITR are affixed to the posts extending medially and laterally from the knee (D) Sagittal view of the tibial fixture mounted on a specimen.

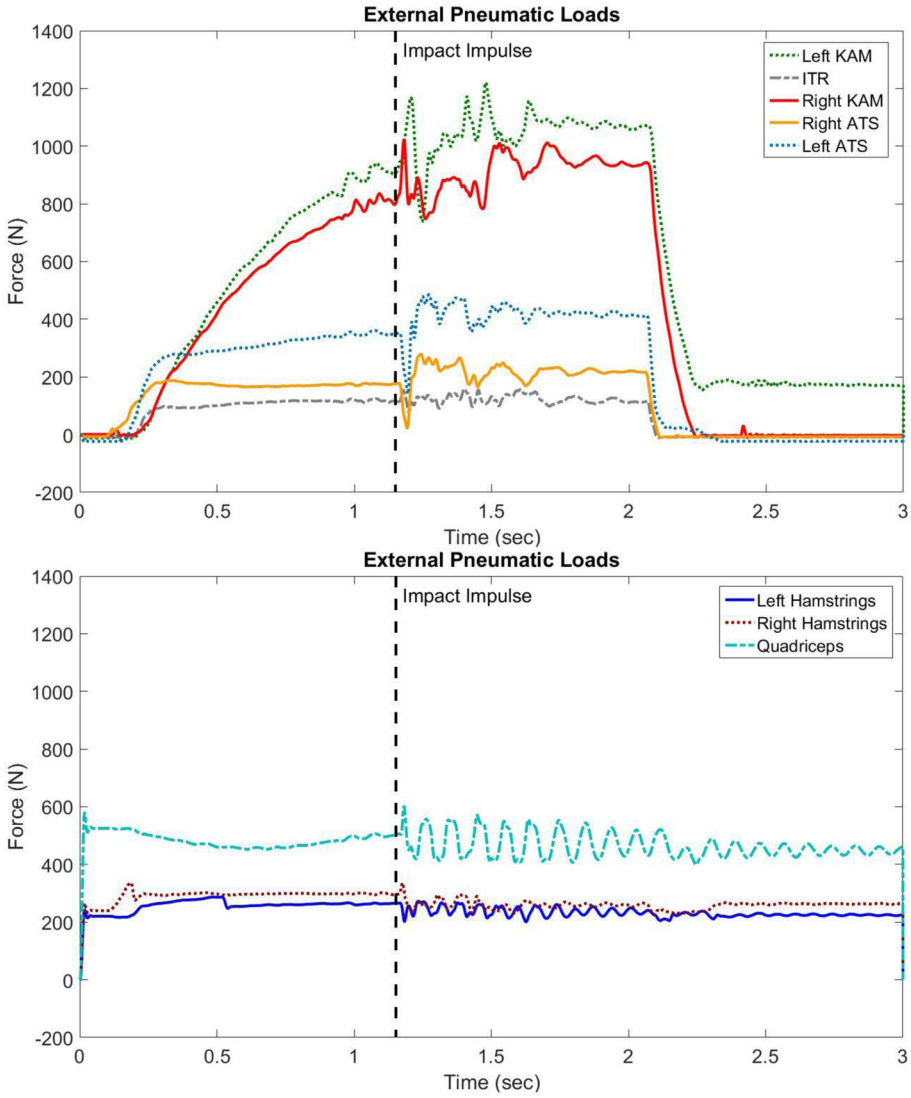

Figure 3.

Plot of force against time as recorded by uniaxial load cells mounted on the ends of each pneumatic cylinder for (A) representive behaviors for pneumatic actuation of external KAM, ATS, and ITR during an impact simulation, and (B) representive behaviors for pneumatic muscle tendon activation during an impact simulation. Though the hamstrings and quadriceps cylinders are loaded at a constant magnitude throughout each trial, the additional dynamic elements in this model can cause fluctuation in how that force is propogated to the specimen. The magnitudes presented were in response to 100% loading in each KAM, ATS, and ITR.

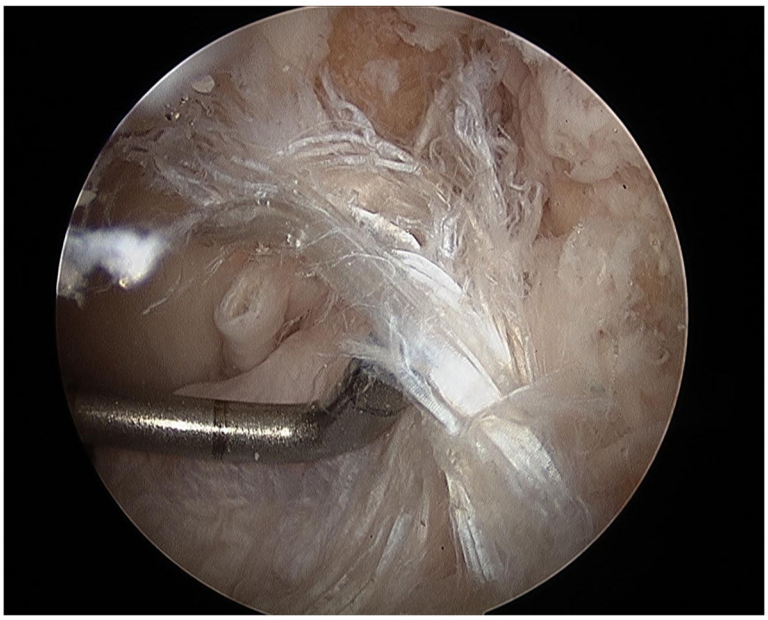

Figure 4.

Image of an ACL rupture that was induced with the mechanical impact simulator. The complete disruption of proximal fibers of the ACL from the femoral origin (superior aspect of image) is visible. The tibial aspect of the ligament remains intact (inferior aspect of image). This pattern is representative of clinically-observed ACL disruptions.

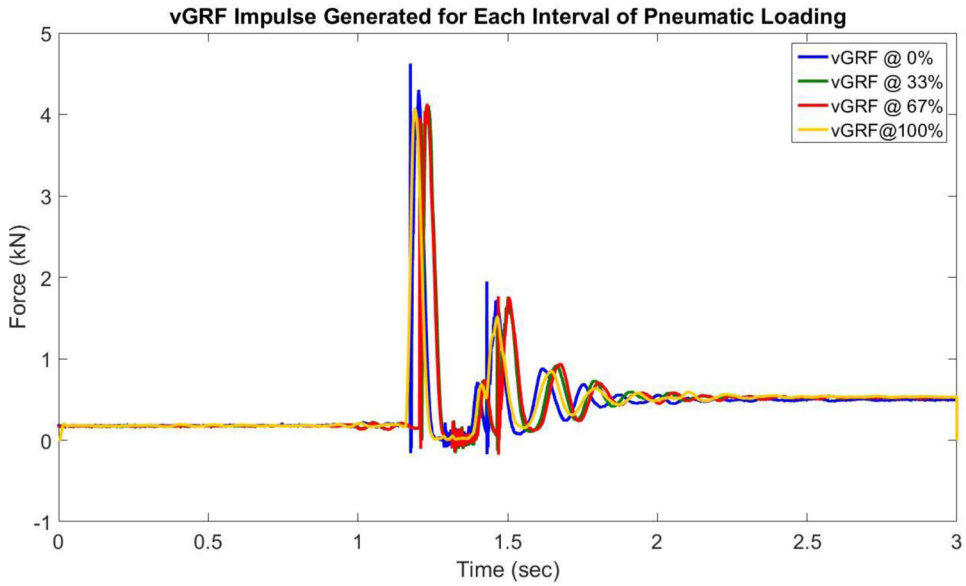

Figure 5.

Depiction of vGRF impulse (in lbs.) induced on the uniaxial load cell contained within the "ground" weight sled. Regardless of what external loads were applied to the specimen this impulse was consistent throughout testing. Therefore, there were no confounding effects of impulse magnitude.

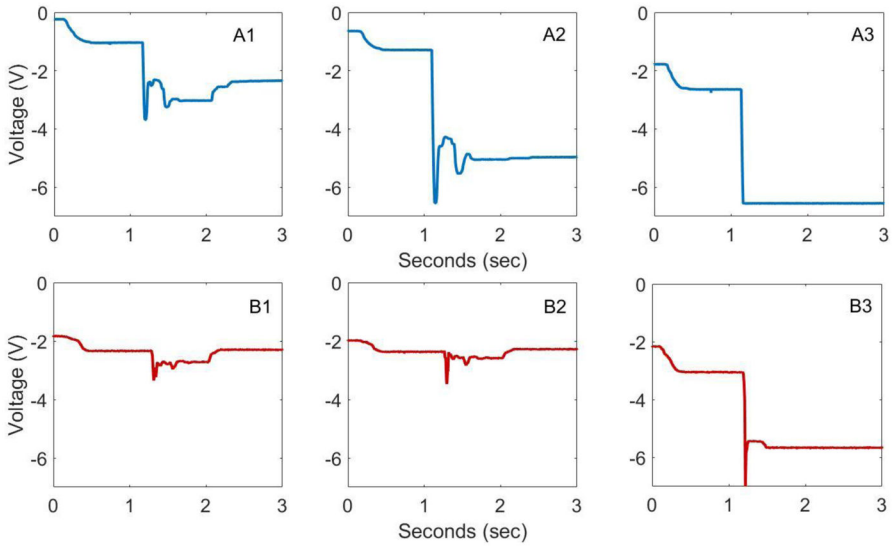

Figure 6.

Progression of DVRT voltage reading through ACL rupture. Panel (A) depicts a subject where partial damage is suspected in the impact immediately prior to complete ACL injury. This is seen as the ligament strain in A2 only rebounds to a magnitude that is significantly larger than the peak magnitude of A1. Such behavior is indicative of a loss in elastic behavior from the ligament fibers. Panel (B) depicts a subject where no partial damage was suspected. Note that decreasing DVRT voltage correlates to increasing ligament strain.

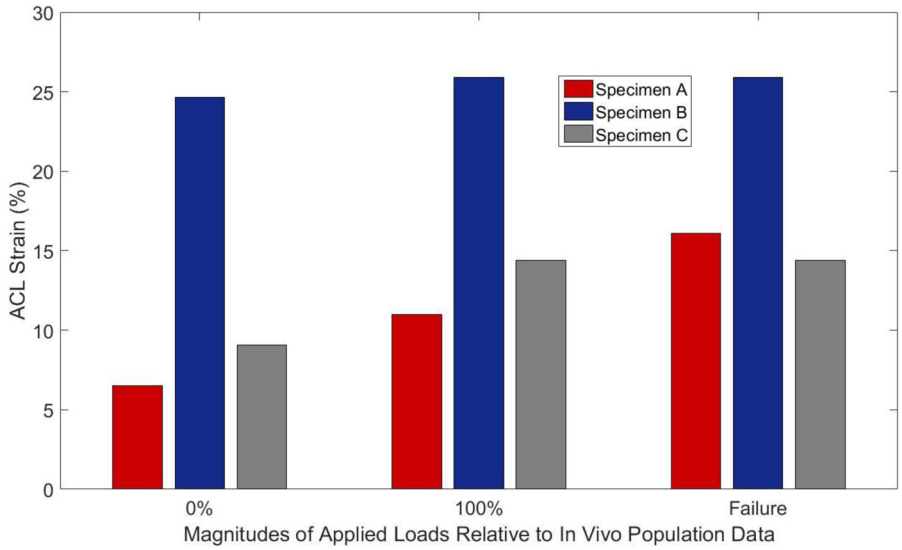

Figure 7.

Depiction of peak strain generated in the ACL of each specimen during impact testing as recorded by implanted DVRT sensors. Peak strain is reported for external pneumatic loads designed to mimic the 0th percentile of *in vivo* data, 100th percentile of *in vivo* data, and the impact immediately preceding specimen failure.

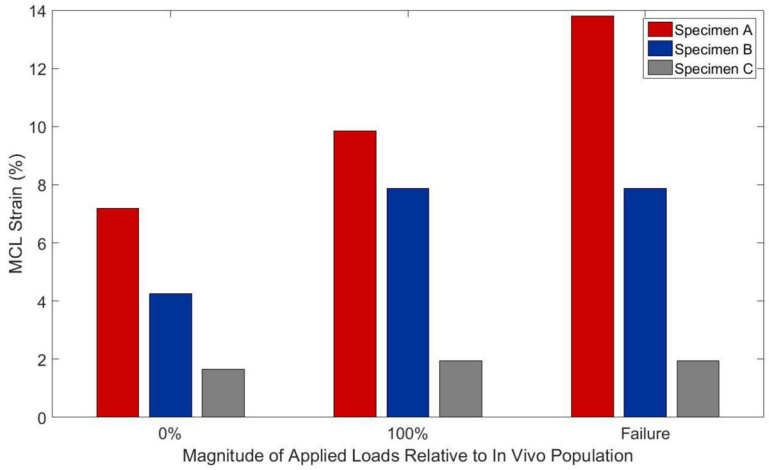

Figure 8.

Depiction of peak strain generated in the MCL of each specimen during impact testing as recorded by implanted DVRT sensors. Peak strain is reported for external pneumatic loads designed to mimic the 0th percentile of *in vivo* data, 100th percentile of *in vivo* data, and the impact immediately preceding specimen failure.

Table 1

KAM, ITR, and ATS load magnitudes based on *in vivo* population percentage.

Population Percentage	KAM (Nm)	ITR (Nm)	ATS (N)
0%	1.7	1.0	47
33%	13.5	9.7	64
67%	26.8	18.6	80
100%	57.3	53.7	196

Table 2

Protocol for impact loading conditions.

SUB-FAILURE PROTOCOL					FAILURE PROTOCOL				
Test	**KAM %**	**ITR%**	**ATS%**	**Drop**	**Test**	**KAM %**	**ITR%**	**ATS%**	**Drop**
1	0%	0%	0%	34.0 kg	1	100%	100%	100%	0.5*BW
2	0%	0%	33%	34.0 kg	2	120%	120%	120%	0.5*BW
3	0%	33%	0%	34.0 kg	3	140%	140%	140%	0.5*BW
4	0%	33%	33%	34.0 kg	4	160%	160%	160%	0.5*BW
5	33%	0%	0%	34.0 kg	5	180%	180%	180%	0.5*BW
6	33%	0%	33%	34.0 kg	6	200%	200%	200%	0.5*BW
7	33%	33%	0%	34.0 kg	7	220%	220%	220%	0.5*BW
8	33%	33%	33%	34.0 kg	8	240%	240%	240%	0.5*BW
9	0%	67%	0%	34.0 kg	9	260%	260%	260%	0.5*BW
10	0%	67%	33%	34.0 kg	10	280%	280%	280%	0.5*BW
11	33%	67%	0%	34.0 kg	11	300%	300%	300%	0.5*BW
12	33%	67%	33%	34.0 kg					
13	0%	0%	67%	34.0 kg					
14	0%	33%	67%	34.0 kg					
15	33%	0%	67%	34.0 kg					
16	33%	33%	67%	34.0 kg					
17	67%	0%	0%	34.0 kg					
18	67%	0%	33%	34.0 kg					
19	67%	33%	0%	34.0 kg					
20	67%	33%	33%	34.0 kg					
21	0%	67%	67%	34.0 kg					
22	33%	67%	67%	34.0 kg					
23	67%	67%	0%	34.0 kg					
24	67%	67%	33%	34.0 kg					
25	67%	0%	67%	34.0 kg					
26	67%	33%	67%	34.0 kg					
27	67%	67%	67%	34.0 kg					

SUB-FAILURE PROTOCOL					FAILURE PROTOCOL				
Test	KAM %	ITR%	ATS%	Drop	Test	KAM %	ITR%	ATS%	Drop
28	33%	100%	33%	34.0 kg					
29	33%	100%	67%	34.0 kg					
30	67%	100%	33%	34.0 kg					
31	67%	100%	67%	34.0 kg					
32	33%	33%	100%	34.0 kg					
33	33%	67%	100%	34.0 kg					
34	67%	33%	100%	34.0 kg					
35	67%	67%	100%	34.0 kg					
36	100%	33%	33%	34.0 kg					
37	100%	33%	67%	34.0 kg					
38	100%	67%	33%	34.0 kg					
39	100%	67%	67%	34.0 kg					
40	33%	100%	100%	34.0 kg					
41	67%	100%	100%	34.0 kg					
42	100%	100%	33%	34.0 kg					
43	100%	100%	67%	34.0 kg					
44	100%	33%	100%	34.0 kg					
45	100%	67%	100%	34.0 kg					
46	100%	100%	100%	34.0 kg					

Note: These tests would be cluster randomized as described.

Table 3

Clinical exam grades and rupture anatomy for each specimen after failure testing.

Specimen	Lachman	Anterior Drawer	Posterior Drawer	MCL	ACL Tear Location	Additional Injuries
A	3	3	0	2	AM femoral avulsion, PL partial mid-substance	MCL anatomically intact, but suspicion of functional damage
B	3	3	0	3	AM femoral avulsion, PL mid- substance	Chondrocalcinosis; MCL anatomically intact, but suspicion of functional damage
C	3	3	0	2	AM femoral avulsion, PL partial mid-substance	MCL anatomically intact, but suspicion of functional damage